Mitochondrial respiratory function as an early biomarker of apoptosis induced by growth factor removal

Hélène Lemieux[1,¤,*], Patrick Subarsky[2], Christine Doblander[1], Martin Wurm[1], Jakob Troppmair[1] and Erich Gnaiger[1,2,*]

[1]Daniel Swarovski Research Laboratory, Department of Visceral, Transplant and Thoracic Surgery, Medical University Innsbruck, Innsbruck, Austria; [2]Oroboros Instruments, Innsbruck, Austria; [¤]Current address: Faculty Saint-Jean, Department of Medicine, Women and Children's Health, Research Institute, University of Alberta, Edmonton, Alberta, Canada

Running title: **Mitochondrial respiratory function as a biomarker of apoptosis**

Keywords: Mitochondrial respiration, OXPHOS, cytochrome *c* oxidase, apoptosis, CRAF, interleukin 3

*Shared corresponding authors

Correspondence:

Erich Gnaiger
Daniel Swarovski Research Laboratory
Department of Visceral, Transplant and Thoracic Surgery
Medical University of Innsbruck
Innrain 66/4
6020 Innsbruck
Austria
Phone: +43 512 566796
Fax: +43 512 566796 20
Email: erich.gnaiger@oroboros.at

Hélène Lemieux
Faculty Saint-Jean,
Dept. of Medicine
Women and Children's Health Research Institute
University of Alberta,
8406, Marie-Anne-Gaboury Street (91 street)
Edmonton, Alberta,
T6C 4G9
Canada
Phone: 1-780-465-8738
Fax: 1-780-465-8760
Email: helene.lemieux@ualberta.ca

Abstract
Intracellular signaling pathways not only control cell proliferation and survival, but also regulate the provision of cellular energy and building blocks through mitochondrial and non-mitochondrial metabolism. Wild-type and oncogenic RAF kinases prevent apoptosis following the removal of interleukin 3 (IL-3) from mouse pro-myeloid 32D cells by reducing mitochondrial reactive oxygen species production. To study primary effects of RAF on mitochondrial energy metabolism, we applied high-resolution respirometry after short-term IL-3 deprivation (8 h), before 32D cells show detectable signs of cell death. Respiration in living 32D cells was suppressed as an early event following removal of IL-3, but remained more stable in 32D cells expressing the v-RAF oncogene. In permeabilized 32D cells deprived of IL-3, succinate-supported respiration remained unchanged, but respiratory capacities of the NADH-pathway and the convergent NS-pathway (NADH-linked substrates in combination with succinate, reconstituting tricarboxylic acid cycle function) were decreased compared to cells grown in the presence of IL-3. This was consistent with respiratory control exerted by the impaired Complex IV activity, since the apparent excess Complex IV capacity was zero above NS-pathway capacity. In comparison, electron flow reached only 60% when supported by succinate alone through Complexes II, III and IV, and was therefore relatively insensitive to Complex IV injuries up to a threshold of 40% inhibition. After IL-3 depletion respiration increased by 15% following addition of cytochrome *c*, which is a marker of mitochondrial outer membrane leakage thus indicating mitochondrial fragility. Our results highlight a novel link between the key mitogenic and survival kinase CRAF and mitochondrial energy homeostasis.

Introduction

RAF serine-threonine kinases are evolutionary highly conserved components of cellular signal transduction, which promote cell growth, transformation and survival [1, 2]. The RAF kinase family comprises the originally identified viral oncogene v-RAF and the subsequently cloned proto-oncogenes CRAF, ARAF and BRAF [3]. In melanoma, the activation of the mitogen-activated protein kinase pathway by BRAF mutants has been shown to be the primary cause of malignant transformation [4]. Furthermore, treatment with BRAF inhibitors significantly improves the survival of patients with metastatic melanoma [4, 5].

The anti-apoptotic function of CRAF is well documented by overexpression and gene knockout studies [6]. Cell death is increased in CRAF and BRAF deficient animals [7-12]. The mitochondrion is a key organelle involved in the regulation of apoptosis. Studies on the control of cell survival by CRAF suggest a role for this kinase in maintaining mitochondrial (mt) integrity and counteracting induction of apoptosis (reviewed by [6]). In vascular endothelial cells, fibroblast growth factor induces CRAF translocation and its binding to mitochondria through the N-terminal domain (reviewed by [13]). Oridonin significantly inhibit the Ras/Raf signaling pathway in an oesophageal cancer xenograft mouse model, inducing mitochondria-dependent apoptosis and markedly inhibiting tumor growth [14]. In addition, cells are protected from apoptosis when RAF accumulates in the mitochondria [9, 15, 16].

Crosstalk between mitochondria and other compartments of the cell has important regulatory functions and is mediated by small molecules, such as reactive oxygen species (ROS) and Ca^{2+}, and by components of intracellular signaling pathways [17-19]. Oncogenically activated signaling proteins are implicated in the metabolic rewiring of tumor cells including the well-established shift from oxidative phosphorylation to glycolysis under normoxic condition [4, 20, 21]. Thus the frequently mutated RAS oncogene, an essential upstream component in the activation of RAF kinases, exerts many effects on mitochondria including an increase in mt-mass, mtDNA content [22], concentrations of tricarboxylic acid (TCA) cycle intermediates [23], and modifications of mt shape and distribution [15]. Furthermore, RAS, located upstream of RAF protein in the RAS/RAF/MEK pathway, is linked to an increase in

mt-production of ROS [22, 24, 25]. K-RAS protein is localized to the mitochondria and causes mt-respiratory dysfunction at an early time point [26]. In fact, more than a third of human tumors present an activated mutant RAS oncogene [27, 28].

Small GTPases of the RAS family have effectors other than RAFs. Some studies demonstrate increased ROS levels in cells transformed by RAS [25], whereas RAF-transformed cells upregulate defense mechanisms by increasing antioxidant capacity [29, 30]. In hepatocellular carcinoma cells resistant to treatment by the multikinase inhibitor sorafenib also targeting RAF, activating oxidative phosphorylation (OXPHOS) by the pyruvate dehydrogenase kinase inhibitor dichloroacetate markedly sensitizes the cancer cells to apoptosis [31, 32]. A similar observation has been reported for melanoma cells carrying the activating V600E mutation in BRAF [20]. Mutant BRAF in melanoma cells downregulates expression of PGC1α, a member of the superfamily of transcriptional co-activators that promote mitochondrial biogenesis and enhance OXPHOS (see review [4]). A recent study in pancreatic β cells provides further evidence that the increase in mitochondrial respiration triggered by PKC is in part mediated through CRAF [33]. While these studies illustrate the profound role of RAF kinases in reprogramming tumor cell metabolism and preventing cell death, they do not address a possible direct effect of RAF on OXPHOS and bioenergetic coupling at earlier time points, which precede the onset of apoptotic cell death.

The goal of our study was to analyze mitochondrial respiratory function after a short absence of growth factor with the known consequences on the shutdown of intracellular signaling cascades, as it may occur *in vivo* during stroke or ischemia/reperfusion in solid organ transplantation. Focusing on an early time point, before any molecular signals of apoptosis can be detected, we demonstrated that the significant decline of mitochondrial respiratory capacity is the earliest elucidated effect of growth factor removal. Loss of mt-function was effectively suppressed by oncogenic RAF (v-RAF), suggesting for the first time a direct link between the key mitogenic and survival kinase CRAF and mitochondrial energy homeostasis.

Materials and Methods

Cell culture

Experiments were performed with the parental promyeloid interleukin-3 (IL-3)-dependent cell line 32D and with 32Dv-RAF cells expressing activated CRAF [34, 35]. Cells were grown in RPMI 1640 (PAA Laboratories Pasching, Austria) supplemented with fetal calf serum (10%, heat-inactivated 45 min at 56 °C), 100 U of penicillin (100 $U \cdot mL^{-1}$; Invitrogen, Carlsbad, CA), streptomycin (100 $U \cdot mL^{-1}$; Invitrogen, Carlsbad, CA), L-glutamine (2 mM; Invitrogen, Carlsbad, CA) and WEHI cell-conditioned medium (15%). Every three days cells were split at a ratio of 1:10 and refed with fresh medium. Cell viability was determined by trypan blue exclusion assay and cells were used in experiments only when the viability was above 97%. For starvation experiments cells were washed three times in IL-3 free RPMI 1640 and resuspended in RPMI 1640 without IL-3 at a cell density of $0.5 \cdot 10^6$ $cells \cdot mL^{-1}$ and incubated for 8 h (Fig 1A).

Cell size

Cell volume was analysed in a CASY1 TT cell counter and analyser system (Schärfe System, Reutlingen, Germany) which combines the techniques of particle measurement and pulse area analysis signal processing. Cell suspensions were diluted in isotonic CASY Ton® solution (100 µL in 10 mL) and introduced into the sensor through a capillary. Every cell is recorded with a frequency of 10^6 evaluations per second during the pulse area analysis while passing through the sensor and the individual signals are analysed according to form, width, range and time frame. Events in the range of 6-25 µm diameter were included in the calculation.

Cell cycle analysis

Cells were washed with 3 mL ice cold PBS and the pellet was resuspended in 500 µL ice cold PBS and 5 mL cold absolute ethanol added dropwise. Samples were centrifuged and supernatant was discarded. After a final wash with 5 mL ice cold PBS containing 1% BSA, samples were resuspended in 250 µL DNA staining buffer containing sodium citrate (1 $mg \cdot mL^{-1}$), Triton-X 100 (150 $\mu L \cdot mL^{-1}$), propidium iodide (0.1 $mg \cdot mL^{-1}$) and Ribonuclease A (0.02 $mg \cdot mL^{-1}$) and incubated at 37 °C for 30 min. Propidium iodide fluorescence was measured using linear FL2 channel in a FACSCalibur flow cytometer (Beckton Dickinson) and analyzed using Cellquest software. Resulting peaks corresponded with cell cycle states A, G1, S and G2 [36]. Areas were set to calculate the four peaks in terms of percent of gated events and mean fluorescence intensity.

High-resolution respirometry on living cells

Cell survival was assayed before each experiment by staining with trypan blue. Cell respiration was measured at 37 °C with the Oxygraph-2k (O2k; Oroboros Instruments, Innsbruck, Austria) in 2 mL chambers at a stirrer speed of 750 rpm. Data acquisition and real-time analysis were performed using the software DatLab (Oroboros Instruments, Innsbruck, Austria). Automatic instrumental background corrections were applied for oxygen consumption by the polarographic oxygen sensor and oxygen diffusion into the chamber [37].

The SUIT protocol for respiration in living cells is illustrated in Fig 1B. Respiration of living cells was measured in culture medium RPMI (cell concentration: $1 \cdot 10^6$ $cells \cdot mL^{-1}$) under cellular routine conditions (ROUTINE). After inhibition of ATP-synthase with 2 $\mu g \cdot mL^{-1}$ oligomycin, respiration declined to the resting or leak-compensating state (LEAK). Uncoupling with stepwise titration to an optimal concentration of the protonophore carbonyl cyanide p-(trifluoromethoxy) phenylhydrazone, FCCP, induced maximal respiration as a measure of electron transfer (ET) capacity. Residual oxygen consumption was obtained after inhibition of CI and CIII with 0.5 µM rotenone and 2.5 µM antimycin A (ROX state). Respiration in all states was corrected for residual oxygen consumption and expressed as O_2 flow per cell [38].

FCCP titrations were performed using the Titration-Injection-microPump TIP2k (Oroboros Instruments, Innsbruck, Austria). Two Hamilton syringes fitted with 27 mm needle length and 0.09 mm needle inner diameter were mounted on the TIP2k for simultaneous titration into the two chambers of the O2k. A 10 mM stock solution of FCCP was filled into the Hamilton syringes and 0.1 µL (0.5 µM) step titrations were performed at a titration speed of 20 $\mu L \cdot s^{-1}$. The optimum FCCP concentration for maximal respiratory oxygen flow varied from 3 to 4 µM. Since the uncoupler and inhibitors were dissolved in ethanol, controls were treated with corresponding titrations of ethanol, and no effect was detected.

High-resolution respirometry on permeabilized cells

For the cell permeabilization test and measurement of respiration in permeabilized cells, cells were rinsed twice with mitochondrial respiration medium MiR05 (110 mM sucrose, 60 mM K-lactobionate, 0.5 mM EGTA, 1 $g \cdot L^{-1}$ BSA fatty acid free, 3 mM $MgCl_2$, 20 mM taurine, 10 mM KH_2PO_4, 20 mM K-HEPES, pH 7.1 [39]), and diluted to a concentration of $2 \cdot 10^6$ $cells \cdot mL^{-1}$ in MiR05. The optimum digitonin concentration for selective permeabilization of the plasma membrane was determined in 32D and 32Dv-RAF cells grown in the presence of IL-3 or after 8 h IL-3 withdrawal. ROUTINE-respiration supported by endogenous substrates was measured in MiR05. After addition of rotenone (0.5 µM), succinate (10 mM), and ADP (2.5 mM), digitonin was titrated [40] (Fig 2).

After adding living cells for measurement of ROUTINE-respiration in MiR05 (ce) and permeabilization of cell membranes with optimal digitonin concentration (10 $\mu g \cdot mL^{-1}$), the following substrates, uncoupler and inhibitors were titrated (final concentration in the chamber): glutamate (G; 10 mM), malate (M; 5 mM), and pyruvate (P; 5 mM) as NADH-linked substrates (1PGM); ADP (1 mM), cytochrome *c* (*c*; 10 µM; 2D*c*); succinate (S; 10 mM) as CII-

substrate (3S), FCCP (4U; optimum concentration 3 to 4 µM); rotenone (5Rot; 0.5 µM) and antimycin A (6Ama; 2.5 µM) as CI and CIII inhibitors; ascorbate (0.5 mM) and *N,N,N',N'*-tetramethyl-*p*-phenylenediamine (TMPD; 2 mM) as CIV-linked substrates reducing cytochrome *c*. Chemical background corrections were applied to account for autoxidation of TMPD and ascorbate (in the presence of 280 $U \cdot mL^{-1}$ catalase to prevent accumulation of hydrogen peroxide, which was a linear function of oxygen concentration in the range from 170 to 50 µM [41, 42]).

Enzyme activity, protein assays and reagents

For determination of enzyme activities and protein content, 300 µL cell suspension was pipetted from the O2k chamber at the end of the experiments, snap-frozen in liquid nitrogen and stored at -80 °C until further analysis. Enzyme activities in each samples were assayed in duplicates at 30 °C and expressed in units of $\mu U \cdot cell^{-1}$. U is one µmol of substrate transformed per minute. Citrate synthase activity was measured at 412 nm recording the linear reduction of 0.1 mM 5,5`dithiobis-2-nitrobenzoic acid (ε_{412}: 13.6 $mL \cdot cm^{-1} \cdot \mu mol^{-1}$) in the presence of 0.31 mM acetyl-CoA, 0.5 mM oxaloacetic acid, 0.1 M Tris/HCl, 50 µM EDTA, 5 mM triethanolamine hydrochloride (pH 8.1; [43, 44]). Lactate dehydrogenase (LDH) activity was measured at 340 nm recording the linear decrease of absorbance of 0.3 mM NADH 340 nm (ε_{340} = 6.22 $mL \cdot cm^{-1} \cdot \mu mol^{-1}$) in the presence of 0.25% Triton X-100 (Serva, Vienna, Austria) and 10 mM pyruvate (Fluka, St. Louis, MO, USA, 0.1 M Tris/HCl buffer, pH 7.1 [43]). Protein concentration was determined with the Lowry method (Bio-Rad protein assay kit, Richmond, CA). All chemicals were from Sigma-Aldrich unless specified.

Statistical analysis

The data are presented as medians (min-max). The medians, minimum and maximum values were calculated from averages of 2 technical repeats, or from medians of 4 technical repeats. Comparing means with the medians showed differences <5% without affecting statistical conclusions. Therefore, standard t-tests were used to calculate significance levels between the treatments (with or without IL-3). To determine the effects of addition of cytochrome *c*, or uncoupler, t-tests for dependent samples were used. Significance was considered at $p<0.05$.

Results

Cell survival and protein content are preserved at an early time point of growth factor withdrawal

IL-3 withdrawal from 32D cells (32D-IL3) provides a unique system for the study of cellular alterations that precede the onset of apoptotic cell death. Absence of growth factor for 24 h reproducibly results in apoptosis of 80% of the parental 32D cells and in only 20% of the 32D cells expressing v-RAF (32Dv-RAF cells) [34]. Activated RAF prevents late mitochondrial events preceding cell death, *e.g.*, increase in ROS and mitochondrial Ca^{2+} [29, 30]. The present study focuses on the earliest changes following growth factor removal. IL-3 deprivation for 8 h resulted in no detectable signs of cell death (Fig 1A). Re-addition of IL-3 at the end of the 8-h starvation period prevented subsequent cell death. In all our experiments, the starting cell viability was higher than 96% and remained unchanged after 8 h of IL-3 withdrawal in 32D and 32Dv-RAF cells. A significant decrease in cell volume was observed in 32D cells from 0.79 (0.69-0.93) $pL \cdot cell^{-1}$ to 0.4 (0.83-1.37) $pL \cdot cell^{-1}$, but not in v-RAF protected cells (Table 1). Regardless of the decrease in cell volume, the protein content of 32D and 32Dv-RAF cells was not significantly different after IL-3 withdrawal (Table 1). Furthermore, IL-3 withdrawal for 8 h did not cause detectable effects on cell cycle distribution (Table 2).

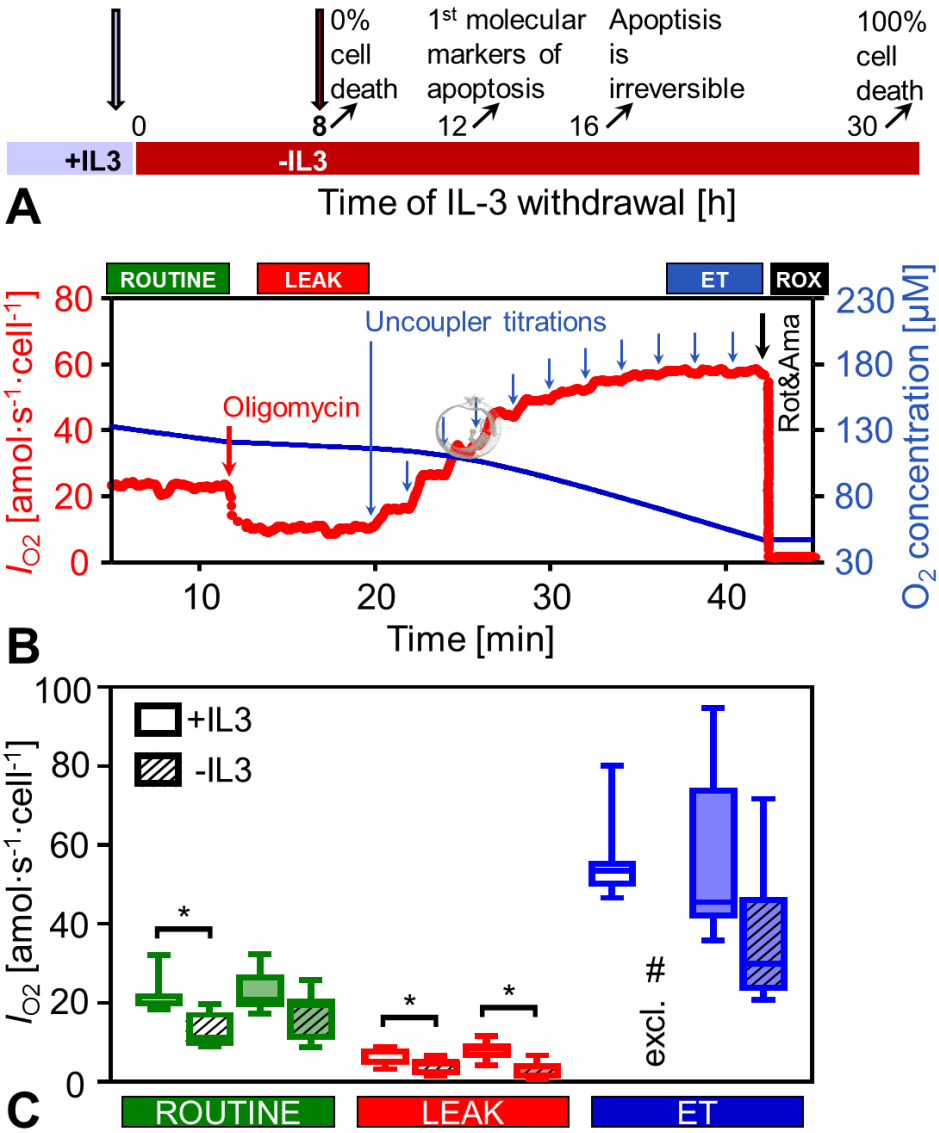

Fig 1: Effect of 8 h IL-3 withdrawal on respiration, I_{O2}, of living 32D and 32Dv-RAF cells. (**A**) Experimental design in the time course of IL-3 withdrawal (-IL3). (**B**) Representative trace of high-resolution respirometry in living 32D cells in the presence of the growth factor IL-3. Oxygen consumption (left axis, bold line) and oxygen concentration (right axis, thin line) are plotted as a function of time of respirometric incubation. Arrows indicate times of titrations in a simple coupling control protocol. Respiration in the ROUTINE-state is O_2 consumption of living cells measured in culture medium (RPMI) which contains exogenous substrates supporting energy metabolism and biosynthesis. Respiration in the LEAK-state is the minimum O_2 consumption compensating mainly for proton leak after inhibition of ATP synthase by oligomycin. Respiratory capacity in the electron transfer-state (ET) is the maximal O_2 consumption at optimum uncoupler concentration. Complexes I and III were inhibited by rotenone and antimycin A for measurement of residual oxygen consumption (ROX-state). Respiration (O_2 flow) is expressed in units of amol O_2 per second per cell. (**C**) Box plots indicate the minimum, 25th percentile, median, 75th percentile, and maximum (n=8 technical repeats; N=3 independent cultures). Left pairs: 32D cells; right pairs: 32Dv-RAF cells. * Significantly different (p<0.05) after IL-3 withdrawal. # A latent injury was revealed in 32D cells when uncoupler titration following oligomycin resulted in respiration not stimulated above the ROUTINE level. Since the actual ET-capacity cannot be lower than ROUTINE-respiration, these data are excluded from the graph (excl.).

Table 1: Cell size, protein content, citrate synthase (CS) and lactate dehydrogenase (LDH) activities in 32D and 32Dv-RAF cells, grown in the presence of IL-3 or after 8 hours of IL-3 withdrawal. Median (min-max), *n*=4-5.

	32D		32Dv-RAF	
	+IL3	-IL3	+IL3	-IL3
Cell volume [pL·cell^{-1}]	0.94 (0.83-1.37)	0.79 (0.69-0.93)*	1.06 (0.99-1.09)	0.90 (0.84-1.16)
Protein content [ng·cell^{-1}]	0.13 (0.06-0.14)	0.17 (0.11-0.27)	0.16 (0.15-0.21)	0.15 (0.11-0.19)
CS activity [µU·cell^{-1}]	0.024 (0.021-0.030)	0.021 (0.015-0.030)	0.029 (0.022-0.045)	0.025 (0.021-0.043)
LDH activity [µU·cell^{-1}]	0.029 (0.018-0.041)	0.023 (0.018-0.038)	0.037 (0.025-0.057)	0.029 (0.023-0.055)

*Significant difference between 32D-IL3 and 32D+IL3; $p<0.05$.

Table 2: Effect of IL-3 starvation on cell cycle distribution of 32D and 32Dv-RAF cells grown in the presence of IL-3 or after 8 h IL-3 withdrawal. Values are means±SD (*n*=5) in percent of cells in each phase of the cycle.

Cell cycle phase	32D		32Dv-RAF	
	+IL3	-IL3	+IL3	-IL3
Sub G0	14±4	14±7	6±3	6±3
G1	53±3	55±4	54±1	55±2
S	8±3	8±5	13±4	13±2
G2	21±2	19±4	23±2	22±3

Activated RAF protects mitochondrial function during growth factor deprivation

ROUTINE-respiration (*R*) of living 32D cells was suppressed significantly after 8 h growth factor deprivation (Fig 1). The decline was not significant in 32Dv-RAF cells (Fig 1C), suggesting that the presence of activated RAF was sufficient to prevent this early change caused by IL-3 withdrawal. Resting oxygen consumption that compensates for proton leak, electron slip and cation cycling (LEAK-respiration, *L*), was measured after inhibition of ATP-synthase with oligomycin (Fig 1B). LEAK-respiration was significantly suppressed in 32D cells after 8 h growth factor deprivation (Fig 1C). The decrease in LEAK-respiration following IL-3 removal, however, was not prevented by v-RAF overexpression. Electron transfer (ET) capacity (*E*) was estimated by uncoupling the cells with optimal concentrations of the protonophore FCCP (Fig 1B). The apparent excess ET-capacity above ROUTINE-respiration, *E-R*, was identical in 32D and 32Dv-RAF cells (Fig 1C). ET-capacity did not decline significantly in 32Dv-RAF cells after IL-3 removal. 32D-IL3 cells, however, presented a latent injury revealed by uncoupler titration after oligomycin treatment, when respiration was unstable and flux was occasionally not even stimulated to the level of ROUTINE-respiration (data not shown). An appropriate estimation of ET-capacity was not possible in those cells after inhibition by oligomycin.

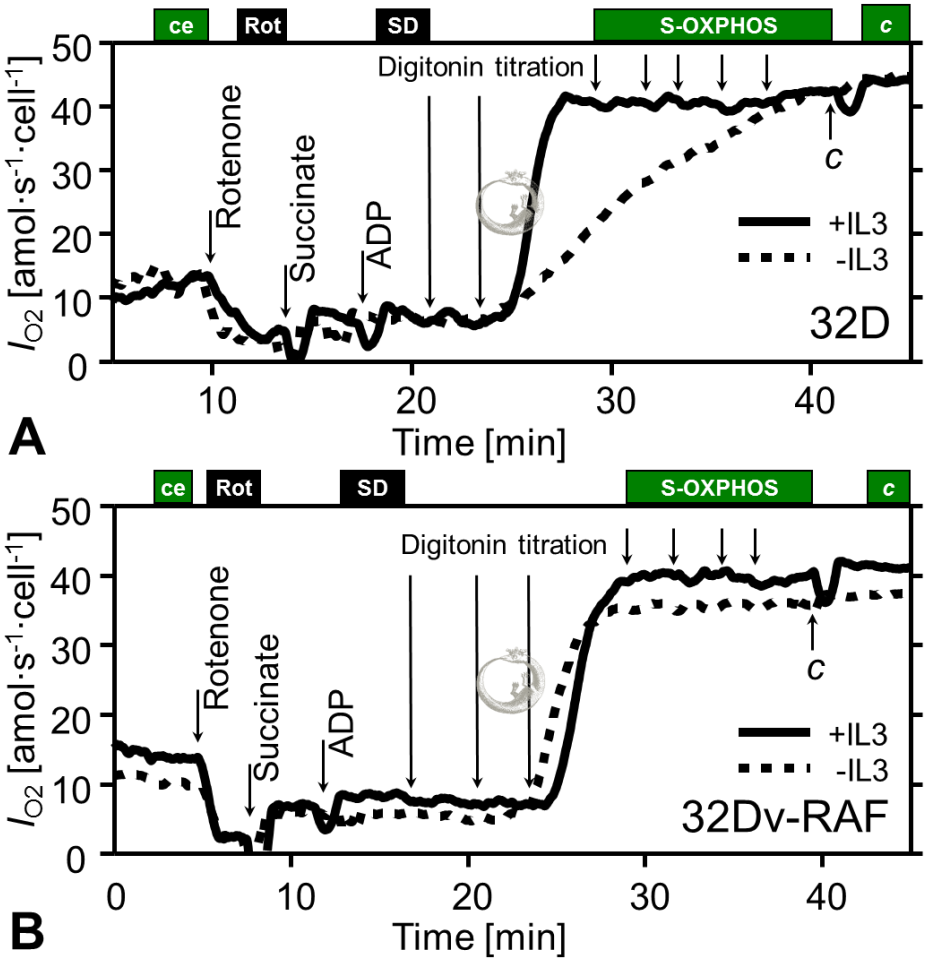

Fig 2: Optimization of digitonin concentration for selective permeabilization of the plasma membrane of 32D cells (**A**) and 32Dv-RAF cells (**B**) in the presence of IL-3 (+IL3; full lines) and after 8 h IL-3 withdrawal (-IL3; dotted lines). Arrows indicate times of titrations. ROUTINE-respiration was recorded after addition of living cells (ce) in MiR05. Rotenone inhibits Complex I (CI), blocks formation of succinate in the TCA cycle and stops simultaneously electron transfer through CII. Thus respiration is inhibited almost completely to the level of residual oxygen consumption (ROX-state). S-OXPHOS capacity is obtained in permeabilized cells after addition of succinate and ADP (SD) and titration of digitonin (concentrations in the chamber: 1, 2, 3, 4, 6, 10 and 20 $mg \cdot L^{-1}$). 10 µM cytochrome *c* (*c*) did not significantly stimulate respiration, indicating that the mitochondrial outer membrane (mtOM) remained intact even at the highest digitonin concentration.

Growth factor deprivation causes defects in OXPHOS- and ET-capacity and cytochrome c release

In order to assess specific defects that cause the decrease in cell respiration after IL-3 removal in the 32D cells, we applied OXPHOS-analysis in permeabilized cells (selectively permeabilizing the plasma membrane). Cells treated with an apoptosis inducer show a change in the sensitivity of the mtOM to digitonin [45]. Therefore, we tested permeabilization of the plasma membrane by digitonin in 32D and 32Dv-RAF cells grown in the presence or absence of IL-3. Cells were incubated in MiR05 in the respiratory ROUTINE-state supported by

endogenous substrates. Rotenone passes the cell membrane, inhibits CI, and inhibits cell respiration immediately. External succinate (S) and ADP are impermeable in living cells and did not stimulate respiration. Digitonin permeabilizes the plasma membrane when titrated above a threshold concentration. Then succinate and ADP become accessible to the mitochondria and respiration is stimulated to the OXPHOS-capacity (*P*) for the S-pathway (Fig 2). The digitonin concentration required for membrane permeabilization was identical in 32D and 32Dv-RAF cells. However, cell membrane permeabilization by digitonin was delayed in 32D-IL3 compared to 32D+IL3 cells, as shown by the slow increase in respiration of the 32D-IL3 cells (Fig 2A, dashed line). In contrast, the time course of cell membrane permeabilization in 32Dv-RAF cells was identical after 8 h with or without growth factor (Fig 2B).

Following optimization of the permeabilization conditions we performed high-resolution respirometry with the objective to diagnose the specific defects of the OXPHOS-system caused by IL-3 withdrawal in 32D cells. The substrate-uncoupler-inhibitor titration (SUIT) protocol is shown in Fig 3A and B. After measurement of ROUTINE-respiration of living cells in MiR05, the plasma membrane was permeabilized by digitonin, and NADH-linked substrates (PGM, supporting the N-pathway) were added to measure LEAK-respiration in the absence of adenylates. OXPHOS-capacity was measured after addition of a saturating concentration of ADP (coupling control). N-LEAK respiration and N-OXPHOS capacity [38] were reduced significantly in 32D-IL3 cells compared to controls (Fig 3C). Cytochrome *c* release was evaluated indirectly by addition of exogenous cytochrome *c* (Fig 3B). No significant stimulation by cytochrome *c* was observed in 32D+IL3 cells. In contrast, the decrease of respiration in 32D-IL3 cells was associated with a small but significant increase in respiration after cytochrome *c* addition. The cytochrome *c* flux control factor, FCF_c = 1 - PGM/*c*PGM, was 0.15 (0.06-0.17), significantly different from zero (paired t-test). After further addition of succinate to support convergent NS-pathway electron flow through CI and CII into the Q-cycle (PGMS), respiration was increased approximately two-fold. The difference between 32D-IL3 and 32D+IL3 cells remained significant (Fig 3C).

Succinate pathway capacity and coupling are preserved during growth factor deprivation

Uncoupler titrations were performed in the presence of the PGMS substrate combination to evaluate NS-ET capacity (*E*; noncoupled [38]) in relation to NS-OXPHOS capacity (*P*; coupled; Fig 3C). An excess *E-P* capacity factor, 1-*P/E*, above 0.0 indicates limitation of OXPHOS-capacity by the phosphorylation system, which is particularly pronounced at maximum ET-capacity supported by convergent NS-electron supply. Even though, uncoupling exerted only a slight effect on NS-pathway capacity. The median excess *E-P* capacity factor was 0.03 (0.02-0.06) and 0.03 (0.01-0.07) in 32D cells, with or without IL-3, respectively. Inhibition of CI by rotenone in the presence of succinate induces the S-pathway control state (Fig 3A). S-ET capacity was not reduced significantly following 8 h IL-3 withdrawal (Fig 3C). S-ET capacity measured in this SUIT protocol agreed with S-OXPHOS capacity obtained in the digitonin titration protocol (Fig. 2).

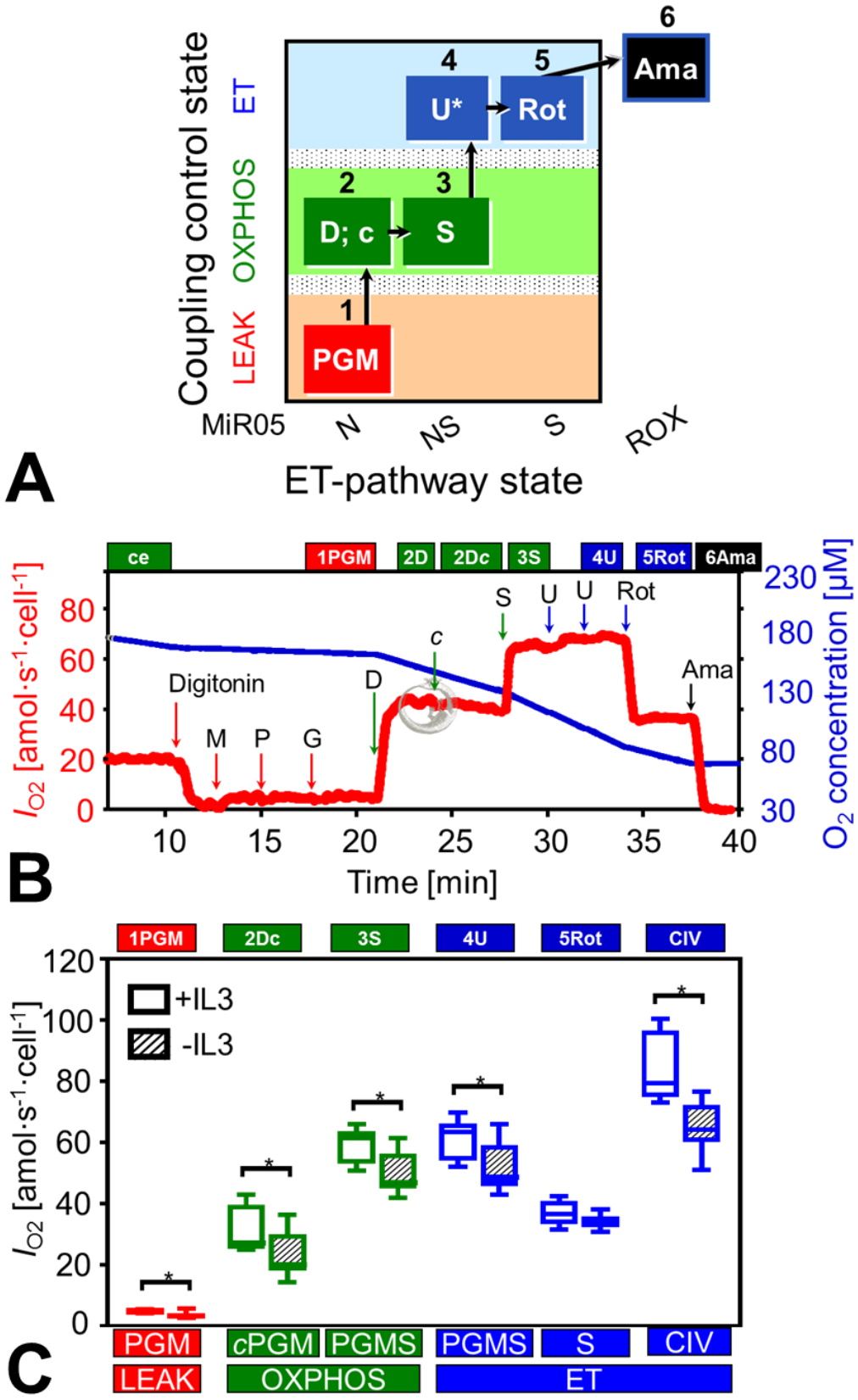

Fig 3: Effect of IL-3 withdrawal on mitochondrial respiration in digitonin permeabilized 32D cells. In the substrate-uncoupler-inhibitor-titration (SUIT) protocol, LEAK-respiration was estimated in the presence of the NADH-linked (N) substrates pyruvate (P), glutamate (G) and malate (M) in the absence of adenylates. OXPHOS-capacity through CI into the Q-junction (N-

pathway; PGM_P) was measured after addition of ADP. Cytochrome *c* (*c*) was added to test the integrity of the mtOM ($_cPGM_P$). Subsequent succinate (S) addition allowed the measurement of respiration with convergent NS-electron flow through CI and CII into the Q-junction ($PGMS_P$). Electron transfer (ET*)* capacity was evaluated by uncoupling with optimum FCCP concentration ($PGMS_E$). Succinate-supported respiration through CII into the Q-junction (S-pathway) was obtained by inhibition of CI with rotenone (Rot). Inhibition of CIII by antimycin A (Ama) provided an estimation of residual oxygen consumption (ROX-state). Cytochrome *c* oxidase activity (CIV) was measured by addition of ascorbate and TMPD and correction of chemical background of autooxidation. (**A**) Coupling/pathway control diagram of the SUIT protocol. The asterisk (4U*) indicates multiple uncoupler titrations. (**B**) Representative experiment showing oxygen flow, I_{O2} (thick line), and oxygen concentration (thin line). Arrows indicate the times of titrations. Cellular ROUTINE-respiration was measured in MiR05 in the absence of exogenous substrates after addition of living cells (ce). Cells were permeabilized with optimum digitonin concentration (10 $mg \cdot L^{-1}$). (**C**) Box plots indicate the minimum, 25^{th} percentile, median, 75^{th} percentile, and maximum (*N*=3 independent cultures; each *n*=4 repeats). * Significantly different ($p<0.05$) after IL-3 withdrawal.

The OXPHOS-coupling efficiency, 1-*L/P* [46], measured in the N-pathway control state with PGM was 0.83 (0.80-0.89) and 0.86 (0.81-0.87), respectively, in control and IL-3 deprived 32D cells (Fig 3). This indicates maintenance of a high degree of coupling. Since OXPHOS-capacity was nearly as high as ET-capacity (Fig 3C), the OXPHOS-coupling efficiency and ET-coupling efficiency, 1-*L/E* [46], are similar. Thus 1-*L/P* in permeabilized cells can be compared with 1-*L/E* in living cells, which was 0.88 (0.84-0.93) in 32D+IL3, 0.84 (0.79-0.89) in 32Dv-RAF+IL3 cells, and 0.91 (0.83-0.98) in 32Dv-RAF-IL3 cells (Fig 1C). Taken together, no dyscoupling (due to mitochondrial injury [38]) occurred prior to apoptosis. Comparable estimates of high coupling efficiency were obtained in permeabilized and living cells, thus indicating that opening of the mt-permeability transition pore was not implicated. Similarly, in human leukemia cells, a high and constant mitochondrial coupling efficiency was observed in the early phase of apoptosis [47].

Complex IV is the main respiratory control variable of mitochondrial injury in 32D cells

Cytochrome *c* oxidase (CIV) is the terminal enzyme in the mitochondrial electron transfer system. Measurement of the enzyme activity of this single step in the pathway of oxygen consumption constitutes a key element in OXPHOS-analysis [48]. After inhibition of CIII by antimycin A, residual oxygen consumption (ROX-state) was close to zero. Ascorbate and TMPD were then added to evaluate CIV activity corrected for autoxidation of ascorbate and TMPD (chemical background). A significant decrease of CIV activity was observed in 32D-IL3 cells compared to control 32D+IL3 cells, similar to the decline of NS-pathway capacity (Fig 3C). Therefore, we determined the threshold level of CIV-capacity by cyanide titrations, as a potential basis to explain the decrease in cell respiration and NS-pathway flux.

OXPHOS-capacity was nearly equivalent to ET-capacity in the NS(PGM) pathway, with *P/E*=0.97 (0.95-0.98) in 32D+IL3 cells and *P/E*=0.97 (0.95-0.97) in 32D-IL3 cells (Fig 3C). Therefore, cyanide titrations were performed in the NS-OXPHOS state which provided higher experimental stability of flux compared to the noncoupled state. Pyruvate was not used in these inhibitor titration experiments, since inhibition of CIV by cyanide is reversed by pyruvate [49]. Cyanide titrations resulted in hyperbolic inhibition of CIV activity and NS-pathway flux (Fig 4A).

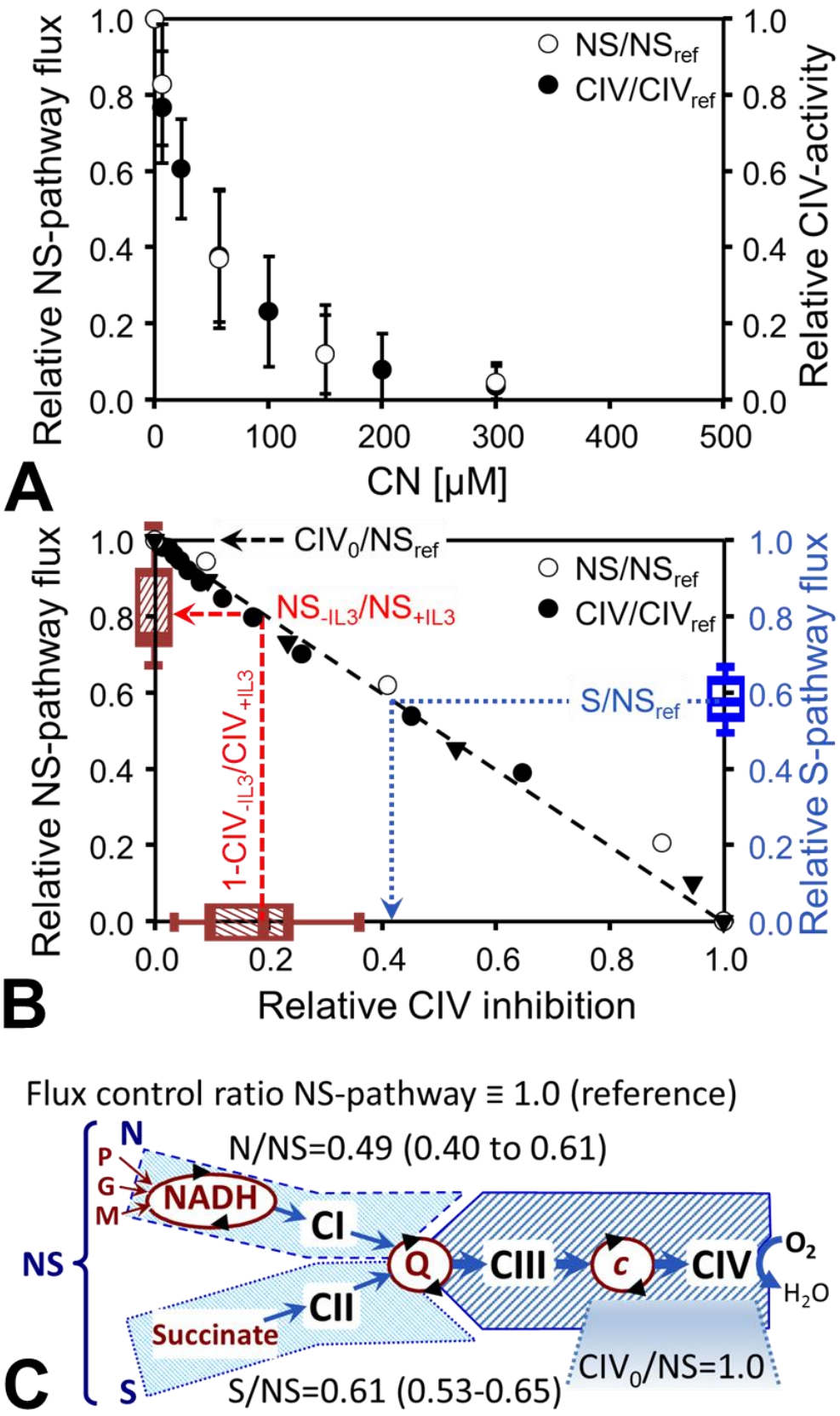

Fig 4: Apparent excess CIV-capacity in 32D cells in relation to diminished NS-pathway capacity after 8 h IL-3 deprivation. (**A**) Permeabilized 32D+IL3 control cells were titrated with cyanide in the presence of glutamate, malate, succinate and ADP (NS; open symbols). NS-pathway flux, NS, is expressed relative to the reference flux at zero inhibitor concentration,

NS_{ref}. Using the same titration steps as in the pathway flux assay, cyanide titrations of CIV enzyme activity (single metabolic step) were performed after inhibition of CI and CIII (rotenone and antimycin A) and stimulation of CIV by ascorbate and TMPD and uncoupler (CIV; filled symbols). CIV-activity, CIV, is expressed relative to the reference CIV-capacity at zero inhibitor concentration, CIV_{ref}. (**B**) Threshold plot for apparent excess CIV-capacity, relating the decline of pathway flux through the electron transfer system to the inhibition of the single enzymatic step of CIV at identical cyanide concentrations. Flux is expressed relative to the reference flux at zero inhibition, NS_{ref}. CIV_0 is calculated as the intercept of the *Y*-axis (at zero CIV inhibition) of a linear regression (dashed line) and expressed as the CIV_0/NS_{ref} flux ratio. The intercept was 1.0. Therefore, the apparent excess CIV-capacity, $j_{ExCIV} = CIV_0/NS_{ref} - 1$, equals zero, representing a zero threshold (for comparison, see [48]). Results are means ± SD (*N*=3 cultures distinguished by different symbols, with duplicate experiments on each culture). CIV inhibition in the -IL3 group after 8 h IL-3 deprivation is plotted on the *X*-axis, expressed relative to +IL3 controls ($1-CIV_{-IL3}/CIV_{+IL3}$; from Fig 3C). NS-pathway capacity in the -IL3 group relative to +IL3 controls is plotted on the left *Y*-axis (NS_{-IL3}/NS_{+IL3}; from Fig 3C). The decline of CIV_{-IL3} capacity thus explains the proportional decline of NS-pathway capacity (dashed line, arrow to NS_{-IL3}/NS_{+IL3}). Preserved S-pathway capacity is fully compatible with the decline of CIV-activity after IL-3 withdrawal, as shown by the flux control ratio for the S-pathway in controls, S/NS_{ref} (+IL3; right *Y*-axis; from Fig 3C), projected onto a threshold of relative CIV inhibition of 0.4 (dotted line, arrow to relative CIV inhibition), which was above the observed CIV_{-IL3} inhibition. (**C**) Schematic representation of the NADH- and succinate- (N and S) pathways converging at the Q-junction, and corresponding N/NS and S/NS flux control ratios in 32D+IL3 control cells, indicating an almost completely additive effect of the converging pathways.

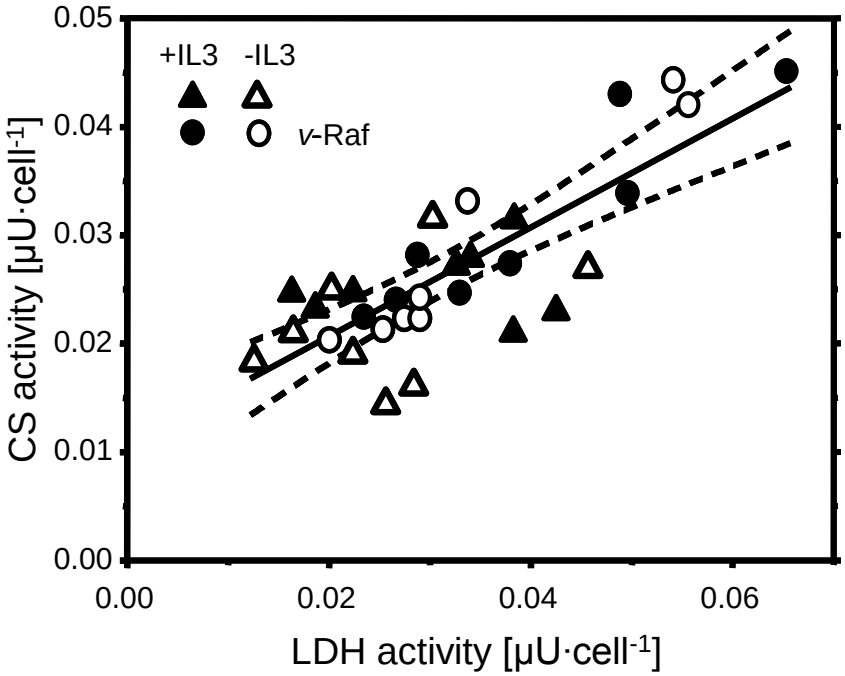

Fig 5: Correlation of the activities of citrate synthase (CS) and lactate dehydrogenase (LDH) expressed per cell.

A threshold plot displays normalized NS-pathway flux (NS/NS_{ref}) as a function of CIV inhibition ($1\text{-}CIV/CIV_{ref}$; Fig 4B). Inhibition of CIV caused a linear, directly proportional inhibition of NS-pathway flux, and the intercept of the linear regression with the *Y*-axis was 1.0. This intercept is the CIV-capacity at zero CIV-inhibition in relation to NS-pathway capacity, CIV_0/NS_{ref}. The excess CIV-capacity is $CIV_0\text{-}NS_{ref}$ with reference to convergent NS-electron flow, or $j_{ExCIV} = CIV_0/NS_{ref}\text{-}1$ when normalized for NS_{ref}. j_{ExCIV} was essentially zero. We analyze in the discussion the implications of zero excess CIV-capacity for interpreting the OXPHOS-flux control pattern in 32D-IL3 cells (Fig 3C).

Constant relation between mitochondrial and glycolytic marker enzyme activites

Activities of the mitochondrial marker enzyme citrate synthase (CS) and the glycolytic marker enzyme lactate dehydrogenase (LDH) expressed per cell did not differ significantly between parental and v-RAF expressing 32D cells and were not significantly reduced by IL-3 deprivation (Table 1). Variations in the activities of these marker enzymes were directly correlated, suggesting no re-programming of glycolytic versus aerobic metabolism under the prevailing growth conditions (Fig 5).

Discussion

Prolonged withdrawal of growth factor (IL-3) results in growth arrest of 32D cells and subsequent apoptosis. After 12 to 15 h of IL-3 deprivation, cells accumulate in the G1 phase, mitochondrial ROS production and mitochondrial Ca^{2+} levels are increased and the cells become irreversibly committed to death at a time point of 16 h [29, 34]. Cell death and the preceding perturbations of mitochondrial Ca^{2+} and ROS homeostasis are delayed by oncogenic v-RAF [29]. The objective of our investigation was to evaluate mitochondrial respiration before the onset of apoptosis. After 8 h IL-3 withdrawal, viability and cell cycle distribution of the 32D cells were not affected, but mitochondrial respiratory capacity was decreased.

To gain insight into the possible mechanisms underlying the reduction of respiratory capacity in IL-3 starved 32D cells, we tested the hypothesis that the change in mitochondrial respiration was caused by a general decrease in mitochondrial content or by a switch from aerobic to glycolytic pathways. A mitochondrial injury causing an increased dependence on glycolysis for ATP production is documented in specific tumors (Warburg effect, see reviews [50-56]). We therefore assayed citrate synthase (CS), an enzyme of the TCA cycle, as a marker of mitochondrial content and lactate dehydrogenase as a glycolytic marker. The results show that the decrease in respiration cannot be explained by an enzymatic switch to glycolysis, since the activities of the two marker enzymes varied in direct proportion, without a significant change following IL-3 withdrawal. Similarly, succinate-supported respiratory capacity did not decline significantly in the 32D-IL3 cells compared to controls. In contrast, N- and NS-pathway capacities and CIV-activity were decreased in 32D cells after 8 h IL-3 withdrawal. A simple diminution of mitochondrial content would affect all mitochondrial pathways at the same proportion, without any change of the pattern of mitochondrial respiratory control. Thus 32D cells show a different pattern compared to leukemia cells where alteration of respiratory capacity and enzyme activities per cell are mainly caused by changes in cell size and mitochondrial content per cell, occurring upon cell cycle arrest triggered by apoptotic agents in the early phase of apoptosis [47].

Our data exclude cell size and mitochondrial content as explanations of the decrease of respiration in living 32D cells after IL-3 withdrawal. Two other possible explanations for the decrease in ROUTINE-respiration are a shift to a metabolic state with lower energy demand, or mitochondrial injuries. Inhibition of respiration by the CI inhibitor rotenone in living cells (Fig 2) is frequently thought to provide a diagnostic measure of electron flow through the NADH-pathway, when rotenone suppresses respiratory activity [26]. This interpretation

ignores the fact that inhibition of CI simultaneously prevents formation of succinate in the TCA cycle. Succinate production is stopped when NADH cannot be oxidized by CI. Without cytosolic sources of succinate, therefore, inhibition of cell respiration by rotenone does not exclusively inhibit electron flux through CI, but simultaneously suppresses the succinate-pathway flux by redox-coupling in the TCA cycle.

In the N-pathway, pyruvate, glutamate and malate dehydrogenases reduce NAD^+ to NADH, feeding electrons into CI. Electrons are further transferred through CIII and CIV to oxygen, the final electron acceptor (N; Fig 4C). CI, CIII and CIV are frequently arranged as supercomplexes [57, 58]. When succinate is provided, electrons are transferred though succinate dehydrogenase (CII) to CIII and CIV (S; Fig 4C). N- and S-pathway capacities were 0.49 and 0.61 of convergent NS-pathway capacity, respectively, thus exerting an almost completely additive effect on the combined pathway (NS; Fig 4C). When measured separately, pathway control resides upstream of the Q-junction, and downstream catalytic capacities are in excess (Fig 4C). When CIV-capacity is in excess, pathway flux does not decrease proportionally to inhibition of CIV-activity due to a threshold effect. In most types of mitochondria, CIV-capacity is in excess of electron transfer pathway capacity, even at maximal upstream electron supply by the convergent NS-pathway [48, 59]. In macrophage cells the apparent excess CIV-capacity, (CIV-NS)/NS, is 0.46 [60]. Similarly, in a variety of human cell lines, the apparent excess CIV-capacity varies between 0.00 and 0.40 in the noncoupled state [61-63]. In 32D cells, the excess CIV-NS capacity was practically zero. This suggests that CIV is the main respiratory control variable of mitochondrial injury in 32D cells. The observation of preserved S-pathway capacity (Fig 3C) does not contradict this conclusion, but provides evidence of a significant excess CIV-capacity with respect to the S-pathway. The corresponding CIV-threshold increases as the S/NS flux control ratio declines [48]. Since the S/NS flux control ratio was as low as 0.6 (Fig 4C), S-pathway capacity is not expected to decline as long as inhibition of CIV does not exceed 40% (Fig 4B). In physiological states with convergent NS-electron flow, the apparent excess capacity of downstream electron transfer is lower and flux control is shifted towards CIII and CIV. An exclusive defect of CIV, however, cannot explain the significant decline of N-OXPHOS capacity, since the N/NS flux control ratio was even lower than S/NS, indicating an additional defect upstream of the Q-junction or in a supercomplex, particularly SC $I_nIII_nIV_n$ (Fig 4C). This is interesting as experimental evidence suggests a role of supercomplex assembly in altering mitochondrial function associated with oncogenic K-Ras [64]. Selective inhibition of CIV in conjunction with exogenous oxidants induces melanoma cell death [65].

Cytochrome *c* normally resides in the mitochondrial inner membrane and is an essential component of the respiratory system, responsible for electron transfer from CIII to cytochrome *c* oxidase [66]. Cytochrome *c* is an important apoptogenic factor, since its release from the mitochondrial intermembrane space initiates caspase activation which leads to apoptotic cell death [67-70]. The respirometric stimulation by addition of exogenous cytochrome *c* is an indirect method to show permeability of the mtOM and release of cytochrome *c* to the cytosol. In the 32D cells deprived of IL-3 for 8 h, cytochrome *c* release was detected to a small extent, without significant increase in cell death or dyscoupling. Mitochondria remained highly coupled even after IL-3 withdrawal, as shown by high OXPHOS-coupling efficiencies in the range of 0.72 to 0.90 measured in the N-pathway control state with PGM. This agrees with results on leukemia cells undergoing apoptosis [47]. Expression of v-RAF residing in the mtOM had also been shown previously to protect 32D cells [71], human leukemia cells [47] and fibroblasts [9] by preventing cytochrome *c* release and subsequent activation of caspases [71]. A possible explanation for the RAF-induced inhibition of cytochrome *c* release in growth factor starved cells is the formation of a complex with the voltage-dependent anion channel (VDAC or porin [71]), a mitochondrial protein involved in the exchange of metabolites for oxidative phosphorylation [72]. The new complex formed *in vivo* blocks reconstitution of VDAC

channels in planar bilayer membranes *in vitro* [71]. It is surprising, however, that cytochrome *c* release was detected at this early time point, when the 32D cells are still not presenting any increase in mortality and can fully recover if they are provided again with IL-3. These findings suggest that the cells deprived of IL-3 may have become more sensitive and experience some mitochondrial membrane fragility.

Our study provides novel insights into a key pathway involved in malignant transformation. Mitochondrial dysfunction is triggered by growth factor limitation, which is a critical step in cancer progression, when the increased size of the growing tumor affects the diffusion of oxygen and nutrients. The viral oncogene v-RAF has been discovered [73] long before mutations were detected in human BRAF [74] and CRAF [1]. The murine homolog BRAF, therefore, might currently be considered as the most relevant oncogene. However, many key findings regarding signaling by oncogenic RAF have been initially obtained with v-RAF and were confirmed later with oncogenic variants of BRAF and CRAF. This suggests that the effects of activated RAF on mitochondrial physiology plays out in human tumors carrying mutant forms of BRAF or CRAF.

Our results demonstrate that IL-3 withdrawal severely compromises mitochondrial respiratory function in a fashion that is suppressible by v-RAF. This suggests a direct link between the key mitogenic and survival kinase CRAF and mitochondrial energy homeostasis. A pro-survival role of mitochondrial respiratory competence is recognized in various types of cancer cells [75-78], indicating that - in contrast to a cancer-specific Warburg effect – changes in mitochondrial respiratory control play a critical role in determining 'positive' or 'negative' fates in both normal and transformed cells. A recent study showed that inhibition of mitochondrial respiration prevent metastasis in BRAF-mutant melanoma [79]. Taken together, these studies suggest that a paradigm shift is required in cancer biology, to avoid biases in interpretation of mitochondrial changes as Warburg-type dysfunctions and open our views to alternative concepts on compensatory or 'adaptive' responses of mitochondrial function in the context of cell metabolism, proliferation, and cell death [80]. The decline of mitochondrial respiratory capacity comprised an early event in the pathway to apoptosis after growth factor withdrawal, before the onset of inactivation of the main signaling effectors of the IL-3 receptor. This time course points to a primary role of mitochondrial respiratory function in apoptosis of these cells.

Author contributions

HL and PS performed the respirometric experiments. CD and MW performed the cell size and cell cycle determinations. EG and JT conceived the project and provided supervision. HL and EG analyzed the data, and wrote the manuscript. JT was responsible for the cell culture and co-wrote the manuscript. EG revised the manuscript.

Competing financial interests

EG is founder and CEO of Oroboros Instruments, Innsbruck, Austria.

Acknowledgments

We thank Tina Goebel for providing technical support for cell culture, Michaela Schneider for performing enzyme activity measurements, and Carolina Doerrier and Javier Iglesias-Gonzalez for helpful discussions. This work was supported by a grant from the Austrian Science Foundation, project MCBO ZFW011010-08, the Austrian Cancer Society/Tyrol, and K-Regio project MitoFit (EG and Oroboros Instruments, Innsbruck, Austria). HL was supported by postdoctoral fellowships from the 'Fonds de Recherche sur la

Nature et les Technologies' (Quebec government, Canada) and the National Sciences and Engineering Council of Canada. Contribution to COST Action CA15203 MitoEAGLE.

References

1. Zebisch A, Troppmair J. Back to the roots: the remarkable RAF oncogene story. Cell Mol Life Sci. 2006;63:1314-30.
2. Zebisch A, Czernilofsky AP, Keri G, Smigelskaite J, Sill H, Troppmair J. Signaling through RAS-RAF-MEK-ERK: from basics to bedside. Curr Med Chem. 2007;14:601-23.
3. Sridhar SS, Hedley D, Siu LL. Raf kinase as a target for anticancer therapeutics. Mol Cancer Ther. 2005;4:677-85.
4. Ratnikov BI, Scott DA, Osterman AL, Smith JW, Ronai ZA. Metabolic rewiring in melanoma. Oncogene. 2017;36:147-57.
5. Ascierto PA, Dummer R. Immunological effects of BRAF+MEK inhibition. Oncoimmunology. 2018;7:e1468955.
6. Troppmair J, Rapp UR. Raf and the road to cell survival: a tale of bad spells, ring bearers and detours. Biochem Pharmacol. 2003;66:1341-5.
7. Wiese S, Pei G, Karch C, Troppmair J, Holtmann B, Rapp UR, et al. Specific function of B-Raf in mediating survival of embryonic motoneurons and sensory neurons. Nat Neurosci. 2001;4:137-42.
8. Wojnowski L, Stancato LF, Zimmer AM, Hahn H, Beck TW. Craf-1 protein kinase is essential for mouse development. Mech Dev. 1998;76:141-9.
9. Zhong J, Troppmair J, Rapp UR. Independent control of cell survival by Raf-1 and Bcl-2 at the mitochondria. Oncogene. 2001;20:4807-16.
10. Huser M, Luckett J, Chiloeches A, Mercer K, Iwobi M, Giblett S, et al. MEK kinase activity is not necessary for Raf-1 function. EMBO J. 2001;20:1940-51.
11. Mikula M, Schreiber M, Husak Z, Kucerova L, Ruth J, Wieser R, et al. Embryonic lethality and fetal liver apoptosis in mice lacking the c-raf-1 gene. EMBO J. 2001;20:1952-62.
12. Liu ES, Raimann A, Chae BT, Martins JS, Baccarini M, Demay MB. c-Raf promotes angiogenesis during normal growth plate maturation. Development. 2016;143:348-55.
13. Tsai Y-T, Chuang M-J, Tang S-H, Wu S-T, Chen Y-C, Sun G-H, et al. Novel Cancer Therapeutics with Allosteric Modulation of the Mitochondrial C-Raf–DAPK Complex by Raf Inhibitor Combination Therapy. Cancer Res. 2015;75:3568-82.
14. Jiang JH, Pi J, Jin H, Cai JY. Oridonin-induced mitochondria-dependent apoptosis in esophageal cancer cells by inhibiting PI3K/AKT/mTOR and Ras/Raf pathways. Journal of cellular biochemistry. 2018.
15. Galmiche A, Fueller J, Santel A, Krohne G, Wittig I, Doye A, et al. Isoform-specific interaction of C-RAF with mitochondria. J Biol Chem. 2008;283:14857-66.
16. Majewski M, Nieborowska-Sorska M, Salomoni P, Slupianek A, Reiss K, Trotta R, et al. Activation of mitochondrial Raf-1 is involved in the antiapoptotic effects of Akt. Cancer Res. 1999;59:2815-9.
17. Guha M, Avadhani NG. Mitochondrial retrograde signaling at the crossroads of tumor bioenergetics, genetics and epigenetics. Mitochondrion. 2013;13:577-91.
18. Hermann M, Kuznetsov A, Maglione M, Smigelskaite J, Margreiter R, Troppmair J. Cytoplasmic signaling in the control of mitochondrial uproar? Cell Commun Signal 2008;6:4.
19. Kröller-Schön S, Steven S, Kossmann S, Scholz A, Daub S, Oelze M, et al. Molecular mechanisms of the crosstalk between mitochondria and NADPH oxidase through reactive oxygen species-studies in white blood cells and in animal models. Antioxid Redox Signal 2014;20:247-66.
20. Haq R, Fisher DE, Widlund HR. Molecular pathways: BRAF induces bioenergetic adaptation by attenuating oxidative phosphorylation. Clin Cancer Res 2014;20:2257-63.

21. Kroemer G, Pouyssegur J. Tumor cell metabolism: cancer's Achilles' heel. Cancer Cell. 2008;13:472-82.
22. Moiseeva O, Bourdeau V, Roux A, Deschênes-Simard X, Ferbeyre G. Mitochondrial dysfunction contributes to oncogene-induced senescence. Mol Cell Biol. 2009;29:4495-507.
23. Ramanathan A, Wang C, Schreiber SL. Perturbational profiling of a cell-line model of tumorigenesis by using metabolic measurements. Proc Natl Acad Sci USA. 2005;102:5992-7.
24. Hlavata L, Aguilaniu H, Pichova A, Nystrom T. The oncogenic RAS2 (val19) mutation locks respiration, independently of PKA, in a mode prone to generate ROS. EMBO J. 2003;22:3337-45.
25. Irani K, Xia Y, Zweier JL, Sollott SJ, Der CJ, Fearon ER, et al. Mitogenic signaling mediated by oxidants in Ras-transformed fibroblasts. Science. 1997;275:1649-52.
26. Hu Y, Lu W, Chen G, Wang P, Chen Z, Zhou Y, et al. K-ras(G12V) transformation leads to mitochondrial dysfunction and a metabolic switch from oxidative phosphorylation to glycolysis. Cell Res. 2012;22:399-412.
27. Gao J, Liao J, Yang GY. CAAX-box protein, prenylation process and carcinogenesis. Am J Transl Res. 2009;1:312-25.
28. Lohr M, Kloppel G, Maisonneuve P, Lowenfels AB, Luttges J. Frequency of K-ras mutations in pancreatic intraductal neoplasias associated with pancreatic ductal adenocarcinoma and chronic pancreatitis: a meta-analysis. Neoplasia. 2005;7:17-23.
29. Kuznetsov AV, Smigelskaite J, Doblander C, Janakiraman M, Hermann M, Wurm M, et al. Survival signaling by C-RAF: Mitochondrial reactive oxygen species and Ca^{2+} are critical targets. Mol Cell Biol. 2008;28:2304-13.
30. Koziel K, Smigelskaite J, Drasche A, Enthammer M, Ashraf MI, Khalid J, et al. RAF and antioxidants prevent cell death induction after growth factor abrogation through regulation of Bcl-2 proteins. Exp Cell Res. 2013;319:2728-38.
31. Shen YC, Ou DL, Hsu C, Lin KL, Chang CY, Lin CY, et al. Activating oxidative phosphorylation by a pyruvate dehydrogenase kinase inhibitor overcomes sorafenib resistance of hepatocellular carcinoma. Br J Cancer. 2013;108:72-81.
32. Bonnet S, Archer SL, Allalunis-Turner J, Haromy A, Beaulieu C, Thompson R, et al. A mitochondria-K+ channel axis is suppressed in cancer and its normalization promotes apoptosis and inhibits cancer growth. Cancer Cell. 2007;11:37-51.
33. Santo-Domingo J, Chareyron I, Dayon L, Núñez Galindo A, Cominetti O, Pilar Giner Giménez M, et al. Coordinated activation of mitochondrial respiration and exocytosis mediated by PKC signaling in pancreatic β cells. FASEB J. 2017;31:1028-45.
34. Cleveland JL, Troppmain J, Packham G, Askew DS, Lloyd P, Gonzalez-Garcia M, et al. v-raf suppresses apoptosis and promotes growth of interleukin-3-dependent myeloid cells. Oncogene. 1994;9:2217-26.
35. von Gise A, Lorenz P, Wellbrock C, Hemmings F, Berberich-Siebelt F, Rapp UR, et al. Apoptosis suppression by Raf-1 and MEK1 requires MEK- and phosphatidylinositol 3-kinase-dependent signals. Mol Cell Biol. 2001;21:2324-36.
36. Vander Heiden MG, Plas DR, Rathmell JC, Fox CJ, Harris MH, Thompson CB. Growth factors can influence cell growth and survival through effects on glucose metabolism. Mol Cell Biol. 2001;21:5899-912.
37. Gnaiger E, Steinlechner-Maran R, Mendez G, Eberl T, Margreiter R. Control of mitochondrial and cellular respiration by oxygen. J Bioenerg Biomembr. 1995;27:583-96.
38. Gnaiger E, Aasander Frostner E, Abdul Karim N, Abumrad NA, Acuna-Castroviejo D, Adiele RC, et al. Mitochondrial respiratory states and rates. MitoFit Preprint Arch. 2019;doi:10.26124/mitofit:190001.v4.
39. Gnaiger E, Kuznetsov AV, Schneeberger S, Seiler R, Brandacher G, Steurer W, et al. Mitochondria in the cold. In: Heldmaier G, Klingenspor M, editors. Life in the cold. New York: Springer Berlin Heidelberg; 2000. p. 431-42.

40. Doerrier C, Garcia-Souza LF, Krumschnabel G, Wohlfarter Y, Mészáros AT, Gnaiger E. High-Resolution FluoRespirometry and OXPHOS protocols for human cells, permeabilized fibers from small biopsies of muscle, and isolated mitochondria. Methods Mol Biol. 2018;1782:31-70.
41. Gnaiger E, Lassnig B, Kuznetsov A, Reiger G, Margreiter R. Mitochondrial oxygen affinity, respiratory flux control and excess capacity of cytochrome *c* oxidase. J Exp Biol. 1998;201:1129-39.
42. Gnaiger E, Steinlechner-Maran R, Méndez G, Eberl T, Margreiter R. Control of mitochondrial and cellular respiration by oxygen. J Bioenerg Biomemb. 1995;27:583-96.
43. Bergmeier HU. Methoden der enzymatischen Analyse. Berlin: Akademie Verlag; 1970.
44. Kuznetsov AV, Strobl D, Ruttmann E, Konigsrainer A, Margreiter R, Gnaiger E. Evaluation of mitochondrial respiratory function in small biopsies of liver. Anal Biochem. 2002;305:186-94.
45. Duan S, Hájek P, Lin C, Shin SK, Attardi G, Chomyn A. Mitochondria outer membrane permeability change and hypersensitivity to digitonin early in staurosporine-induced apoptosis. J Biol Chem. 2003;278:1346-53.
46. Gnaiger E. Mitochondrial pathways and respiratory control. An introduction to OXPHOS analysis. 4th ed. Mitochondr Physiol Network 19.12. Oroboros MiPNet Publications, Innsbruck. 2014:80 pp.
47. Renner K, Amberger A, Konwalinka G, Kofler R, Gnaiger E. Changes of mitochondrial respiration, mitochondrial content and cell size after induction of apoptosis in leukemia cells. Biochim Biophys Acta-Mol Cell Res. 2003;1642:115-23.
48. Lemieux H, Blier PU, Gnaiger E. Remodeling pathway control of oxidative phosphorylation by temperature in the heart. Sci Rep. 2017;7:2840.
49. Nůsková H, Vrbacký M, Drahota Z, Houštěk J. Cyanide inhibition and pyruvate-induced recovery of cytochrome *c* oxidase. J Bioenerg Biomembr. 2010;42:395-403.
50. Dang CV, Semenza GL. Oncogenic alterations of metabolism. Trends Biochem Sci. 1999;24:68-72.
51. Altman BJ, Dang CV. Normal and cancer cell metabolism: lymphocytes and lymphoma. FEBS J. 2012;279:2598-609.
52. Giampazolias E, Tait SW. Mitochondria and the hallmarks of cancer. FEBS J. 2016;283:803-14.
53. Moreno-Sánchez R, Rodríguez-Enríquez S, Marín-Hernández A, Saavedra E. Energy metabolism in tumor cells. FEBS J. 2007;274:1393-418.
54. Villa E, Ricci JE. How does metabolism affect cell death in cancer? FEBS J. 2016;283:2653-26660.
55. Fitzgerald G, Soro-Arnaiz I, Bock K. The Warburg Effect in Endothelial Cells and its Potential as an Anti-angiogenic Target in Cancer. Frontiers in cell and developmental biology. 2018;6:100.
56. Lu J. The Warburg metabolism fuels tumor metastasis. Cancer metastasis reviews. 2019.
57. Acin-Perez R, Enriquez JA. The function of the respiratory supercomplexes: the plasticity model. Biochim Biophys Acta. 2014;1837:444-50.
58. Milenkovic D, Blaza JN, Larsson NG, Hirst J. The Enigma of the Respiratory Chain Supercomplex. Cell Metab 2017;25:765-76.
59. Kunz WS, Kudin A, Vielhaber S, Elger CE, Attardi G, Villani G. Flux control of cytochrome c oxidase in human skeletal muscle. J Biol Chem. 2000;275:27741-5.
60. Groeger M, Matallo J, McCook O, Wagner F, Wachter U, Bastian O, et al. Temperature and cell-type dependency of sulfide effects on mitochondrial respiration. Shock. 2012;38:367-74.
61. Villani G, Greco M, Papa S, Attardi G. Low reserve of cytochrome *c* oxidase capacity *in vivo* in the respiratory chain of a variety of human cell types. J Biol Chem. 1998;273:31829-36.
62. Villani G, Attardi G. *In vivo* control of respiration by cytochrome *c* oxidase in wild-type and mitochondrial DNA mutation-carrying human cells. Proc Natl Acad Sci USA. 1997;94:1166-71.
63. Dalmonte ME, Forte E, Genova ML, Giuffrè A, Sarti P, Lenaz G. Control of respiration by cytochrome *c* oxidase in intact cells: role of the membrane potential. J Biol Chem 2009;284:32331-5.

64. Wang P, Song M, Zeng ZL, Zhu CF, Lu WH, Yang J, et al. Identification of NDUFAF1 in mediating K-Ras induced mitochondrial dysfunction by a proteomic screening approach. Oncotarget. 2015;6:3947-62.
65. Gandhirajan RK, Rodder K, Bodnar Y, Pasqual-Melo G, Emmert S, Griguer CE, et al. Cytochrome *c* oxidase inhibition and cold plasma-derived oxidants synergize in melanoma cell death induction. Sci Rep. 2018;8:12734.
66. Hatefi Y. The mitochondrial electron transport and oxidative phosphorylation system. Ann Rev Biochem. 1985;54:1015-69.
67. Adrain C, Martin SJ. The mitochondrial apoptosome: a killer unleashed by the cytochrome seas. Trends Biochem Sci. 2001;26:390-7.
68. Cain K, Bratton SB, Cohen GM. The Apaf-1 apoptosome: A large caspase-activating complex. Biochimie. 2002;84:203-14.
69. Liu X, Kim CN, Yang J, Jemmerson R, Wang X. Induction of apoptotic program in cell-free extracts: requirement for dATP and cytochrome *c*. Cell. 1996;86:147-57.
70. Zou H, Li Y, Wang X. An APAF-1 cytochrome c multimeric complex is a functional apoptosome that activates procaspase-9. J Biol Chem. 1999;274:11549-56.
71. Le Mellay V, Troppmair J, Benz R, Rapp UR. Negative regulation of mitochondrial VDAC channels by C-Raf kinase. BMC Cell Biol. 2002;3:14.
72. Colombini M, Blachly-Dyson E, Forte M. VDAC, a channel in the outer mitochondrial membrane. In: Narahashi T, editor. Ion channels. 4. New York: Plenum Publishing Corp.; 1996. p. 169-202.
73. Rapp UR, Goldsborough MD, Mark GE, Bonner TI, Groffen J, Reynolds FH, Jr., et al. Structure and biological activity of v-raf, a unique oncogene transduced by a retrovirus. Proceedings of the National Academy of Sciences of the United States of America. 1983;80:4218-22.
74. Wellbrock C, Karasarides M, Marais R. The RAF proteins take centre stage. Nat Rev Mol Cell Biol. 2004;5():875-85.
75. Tan AS, Baty JW, Dong LF, Bezawork-Geleta A, Endaya B, Goodwin J, et al. Mitochondrial genome acquisition restores respiratory function and tumorigenic potential of cancer cells without mitochondrial DNA. Cell Metab. 2015;21:81-94.
76. Leucci E, Vendramin R, Spinazzi M, Laurette P, Fiers M, Wouters J, et al. Melanoma addiction to the long non-coding RNA SAMMSON. Nature. 2016;531:518-22.
77. Trotta AP, Gelles JD, Serasinghe MN, Loi P, Arbiser JL, Chipuk JE. Disruption of mitochondrial electron transport chain function potentiates the pro-apoptotic effects of MAPK inhibition. J Biol Chem. 2017;doi: 10.1074/jbc.M117.786442.
78. Rodrigues MF, Obre E, de Melo FH, Santos GCJ, Galina A, Jasiulionis MG, et al. Enhanced OXPHOS, glutaminolysis and β-oxidation constitute the metastatic phenotype of melanoma cells. Biochem J. 2016;473:703-15.
79. Sundstrom T, Prestegarden L, Azuaje F, Aasen SN, Rosland GV, Varughese JK, et al. Inhibition of mitochondrial respiration prevents BRAF-mutant melanoma brain metastasis. Acta neuropathologica communications. 2019;7:55.
80. Bajzikova M, Kovarova J, Coelho AR, Boukalova S, Oh S, Rohlenova K, et al. Reactivation of dihydroorotate dehydrogenase-driven pyrimidine biosynthesis restores tumor growth of respiration-deficient cancer cells. Cell Metab. 2019;29:399-416.